the plant journal

SEB SOCIETY FOR EXPERIMENTAL BIOLOGY

The Plant Journal (2025) **121,** e17238 doi: 10.1111/tpj.17238

Extensive remodeling during *Chlamydomonas reinhardtii* zygote maturation leads to highly resistant zygospores

Martim Cardador[1], Stephanie Krüger[2], Susanne Dunker[3,4], Alexandra Brakel[5,6], Ralf Hoffmann[5,6], Raimund Nagel[1], Torsten Jakob[1], Reimund Goss[1] and Severin Sasso[1,4,*]

[1]*Institute of Biology, Leipzig University, Leipzig, Germany,*
[2]*Biozentrum, Microscopy Unit, Martin Luther University Halle-Wittenberg, Halle (Saale), Germany,*
[3]*Helmholtz Centre for Environmental Research (UFZ), Department for Physiological Diversity, Leipzig, Germany,*
[4]*German Centre for Integrative Biodiversity Research (iDiv) Halle-Jena-Leipzig, Leipzig, Germany,*
[5]*Institute of Bioanalytical Chemistry, Leipzig University, Leipzig, Germany, and*
[6]*Center for Biotechnology and Biomedicine, Leipzig, Germany*

Received 22 July 2024; revised 12 November 2024; accepted 18 December 2024.
*For correspondence (e-mail severin.sasso@uni-leipzig.de).

SUMMARY

The unicellular soil alga *Chlamydomonas reinhardtii* forms diploid zygotes during its sexual cycle. The process of a zygote maturing into a highly resistant zygospore remains poorly understood despite its importance for survival under adverse environmental conditions. Here we describe the detailed timeline of morphological and physiological changes during zygote maturation in darkness on ammonium-free Tris-acetate-phosphate agar plates. The formation of a multilayered cell wall is primarily responsible for the increase in cell size in the first few days after zygote formation. Desiccation and freezing tolerance also develop in the period 3–7 days. Photosynthetic and respiratory activity decrease to reach minimal levels after 7–10 days, accompanied by a partial dedifferentiation of the chloroplast that includes chlorophyll degradation followed by the possible disappearance of the pyrenoid. In contrast to the decreasing concentrations of most carotenoids in the first few days after zygote formation, ketocarotenoids can first be detected after 3 days and their accumulation is completed after 10 days. Furthermore, the zygote degrades a large proportion of its starch and enriches oligosaccharides that may serve as osmoprotectants. The storage lipid triacylglycerol is accumulated at the expense of thylakoid membrane lipids, which mirrors the conversion of a metabolically active cell into a dormant spore on the metabolic level. Taken together, zygote maturation is a multifaceted process that yields mature zygospores after ~ 3 weeks. This work sheds light on the complete time course of the remodeling of a photosynthetically active eukaryotic cell into a dormant, highly resistant spore.

Keywords: *Chlamydomonas reinhardtii*, dormancy, spore, zygote ultrastructure, zygospore maturation, desiccation tolerance, freezing tolerance, pyrenoid, carotenoids, electron microscopy.

INTRODUCTION

Chlamydomonas reinhardtii is a unicellular green alga found in temperate soils (Sasso et al., 2018; Ford et al., 2023). It is a formidable model organism to study photosynthesis, motility, the cell cycle, and other fundamental processes (Salomé and Merchant, 2019; Findinier and Grossman, 2023). Many genetic resources are available for *C. reinhardtii*, including a large library of insertional mutants (Li et al., 2019), CRISPR-mediated genome editing (e.g., Akella et al., 2021), a Modular Cloning (MoClo) toolkit (Crozet et al., 2018), and a high-quality genome sequence (Merchant et al., 2007; Craig et al., 2023).

C. reinhardtii profoundly remodels its cell in the course of its life cycle. Haploid vegetative cells possess an eyespot and two anterior cilia that allow directional movement in response to external stimuli (Salomé and Merchant, 2019). A single cup-shaped chloroplast occupies more than half of the cell volume and contains the pyrenoid, an area where CO_2 is concentrated around Rubisco. Vegetative cells can divide asexually by mitosis, and they exist in two mating types, mt^+ and mt^-, which are genetically determined in the mating type locus (Ferris et al., 2002; Goodenough et al., 2023). Sexually competent gametes are induced by nitrogen limitation, and gametes

of opposite mating types can fuse to form diploid zygotes. Over the following days, zygotes can mature into highly resistant, dormant zygospores, which are able to survive freezing, desiccation, and possibly other types of environmental stress (Suzuki and Johnson, 2002; Heimerl et al., 2018). The provision of zygotes with nitrogen induces meiosis to release four haploid cells (germination), which resume vegetative growth to complete the sexual cycle of *C. reinhardtii*. Gametogenesis and germination are regulated by light via different photoreceptors (Huang and Beck, 2003; Müller et al., 2017; Zou et al., 2017). By removing or adding nitrogen and light, the sexual cycle can be easily controlled in the laboratory. In soil, *C. reinhardtii* may utilize these two abiotic factors as signals to perceive deteriorating or improving environmental conditions and adjust its lifestyle accordingly.

A number of molecular factors governing the sexual cycle of *C. reinhardtii* have been elucidated such as ciliary agglutinins or the intracellular signal cyclic adenosine monophosphate (cAMP) (Pasquale and Goodenough, 1987; Ferris et al., 2005). In newly formed zygotes, two homeoprotein transcription factors, GSP1 and GSM1, are contributed by the mt^+ and mt^- gametes, respectively (Kurvari et al., 1998; Lee et al., 2008). GSP1 and GSM1 form a heterodimer and translocate to the nucleus to initiate the zygotic transcription program (Lee et al., 2008). Within minutes after gamete fusion, the first zygote-specific genes are induced, and hundreds of genes follow in the next few hours (Lopez et al., 2015; Joo et al., 2017). Among the genes induced within minutes are *ZSP1* and *ZSP2*, which encode constituent hydroxyproline-rich glycoproteins (HRGPs) of the zygotic cell wall (Woessner and Goodenough, 1989; Suzuki et al., 2000). A 9-bp *cis*-regulatory element has been identified that is enriched in the promoter regions of early zygote genes (Hamaji et al., 2016). The fusion of the two nuclei and the two chloroplasts occurs in the first 2 h, with nuclear fusion preceding chloroplast fusion (Blank et al., 1978). Owing to the selective degradation of organellar DNA, the progeny will inherit the chloroplast genome from the maternal parent (mt^+) and the mitochondrial genome from the paternal parent (mt^-) (Aoyama et al., 2006; Joo et al., 2022). Approximately 3 h after gamete fusion, the zygote starts to resorb its four cilia to become immotile (Pan and Snell, 2005).

In the following maturation period, the zygote assembles a resistant cell wall consisting of approximately six layers (Cavalier-Smith, 1976; Grief et al., 1987). As in vegetative cells, HRGPs are major components of the zygotic wall, but the set of HRGPs differs between zygotes and vegetative cells (Woessner and Goodenough, 1989; Goodenough and Lee, 2023). Zygotes also degrade chlorophyll and accumulate storage products while maturing into dormant zygospores (Cavalier-Smith, 1976). A gene with a predicted size of 83 kb, *PKS1*, is involved in cell wall formation and is essential for desiccation tolerance (Heimerl et al., 2018). As shown in the accompanying article by Schwarz et al., (2025) a β-carotene ketolase encoded by *BKT* catalyzes the formation of secondary ketocarotenoids in zygotes. However, compared with the number of genes with known roles during gametogenesis and the first few hours of zygote development, the remodeling of early zygotes into mature zygospores remains largely unexplored.

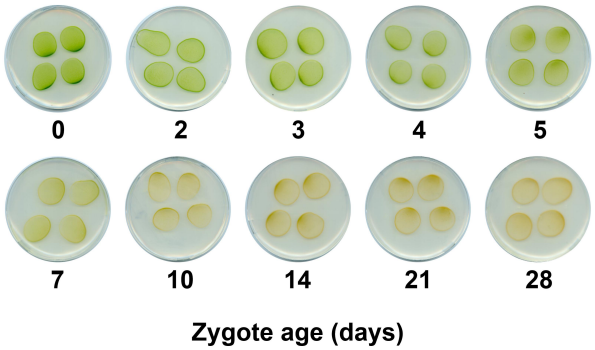

Figure 1. Change of pigmentation during the maturation of *C. reinhardtii* zygotes. Aliquots of zygotes were matured for 4 weeks on ammonium-free TAP-N plates in the dark.

Here, we systematically monitor zygote maturation in *C. reinhardtii* on several structural and functional levels over 4 weeks and reveal an extensive morphological and physiological remodeling of zygotes. We show that the development of zygotes into zygospores is a complex multi-stage process that consists of multiple sequential and partly overlapping processes.

RESULTS

Zygote maturation leads to cell enlargement and further morphological changes

Our experiments were designed to systematically study the maturation of zygotes into zygospores in darkness on TAP agar plates without ammonium chloride (TAP-N plates). Initially, green zygotes began to turn yellow after 7 days of maturation and their color intensified to orange over the following week (Figure 1). No further color change was apparent after 14 days. The observation that *C. reinhardtii* zygotes undergo such a dramatic change in a short period of time raised our interest to delve deeper into the morphological and physiological changes that accompany zygote maturation.

Scanning electron microscopy (SEM) of mature zygospores revealed nearly spherical cells with essentially smooth surfaces (Figure 2a; Figure S1A). To the best of our knowledge, no SEM images of *C. reinhardtii* zygospores have been published. The SEM observations are supported by transmission electron microscopy (TEM) as all the sectioned zygospores displayed smooth surfaces once the cell

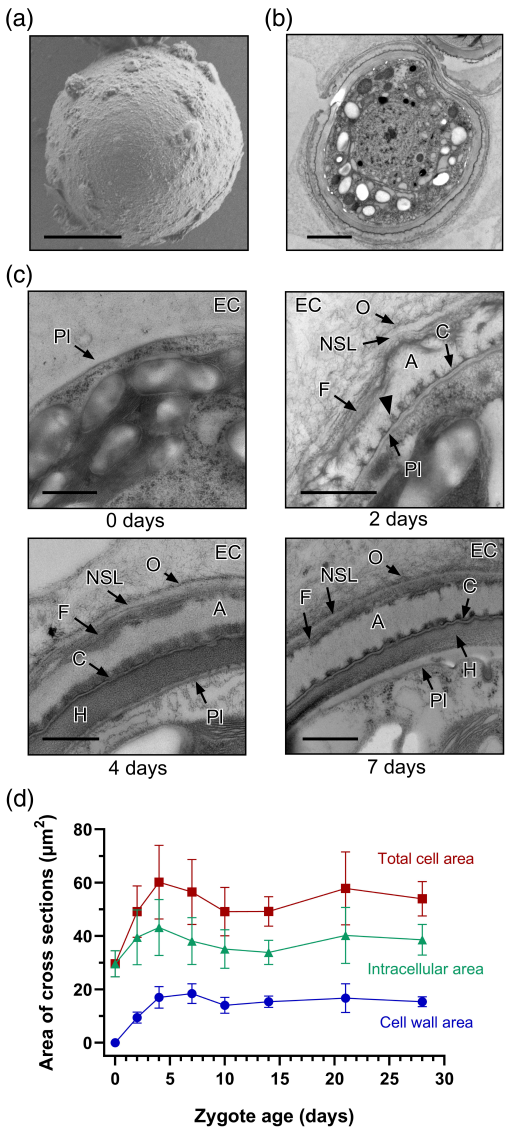

Figure 2. Electron micrographs of mature zygospores and cell wall assembly during zygote maturation. Zygotes were matured on ammonium-free TAP-N plates in the dark. (a) Scanning electron micrograph of a mature zygospore (4 months old). Scale bar: 4 μm. (b) TEM image of the intracellular ultrastructure of a mature zygospore (2 months old). Scale bar: 2 μm. (c) Temporal stages of the developing cell wall. Scale bar: 0.5 μm. The arrowhead highlights a knob associated with the nascent central layer after 2 days. The cell wall layers are named according to Grief et al. (1987): A, alveolate layer; C, central layer; EC, extracellular environment; F, fibrous layer; H, homogeneous layer; NSL, non-staining layer; O, outer, fibrous pellicle material; Pl, plasma membrane. (d) Quantification of total cell area, intracellular area, and cell wall area in TEM cross-sections. Values indicate the mean ± standard deviation, with n = 16–24 (number of cells analyzed).

wall was fully developed (Figure 2b; see also Figure S4). To further validate our findings, we examined the cells using environmental scanning electron microscopy (ESEM), which in contrast to SEM and TEM does not require dehydration or any other pre-treatment of the samples that may alter the morphology of the cells. ESEM confirmed that mature zygospores are smooth, spherical cells (Figure S1b).

TEM provided further information on the development of the zygotic cell wall during maturation. For TEM and all subsequent experiments, newly formed zygotes (t = 0) were analyzed or processed 3–6 h after their formation. These zygotes were devoid of a cell wall (Figure 2c), which is in line with the observation that gametes shed their cell walls before they fuse (Cavalier-Smith, 1975). Two days after zygote formation, an immature cell wall with poorly defined layers was visible. Nevertheless, five of the six layers described by Grief et al. (1987), can be recognized at this stage of maturation. As can be seen from the electron-dense knobs, which may be a polymerization intermediate of the central layer (also called the *central lamina*; Heimerl et al., 2018), this layer is currently being formed (Figure 2c). The homogenous layer, which is the innermost layer in mature zygospores, is still missing in 2-day-old zygotes but present after 4 days. With increasing maturation time, the borders between the layers became more clearly defined (Figure 2c). After more than 7 days, no substantial changes to the cell wall structure were observed (Figure S2).

To assess whether the formation of the multilayered cell wall results in an increase in zygote size, the area in TEM cross-sections was quantified. While the intracellular area remained fairly constant, the increase in cell wall area in the first 4 days paralleled the increase in total cell size (Figure 2d), suggesting that the synthesis of the cell wall is the main driver of the size increase. To further validate these findings, we employed imaging flow cytometry (IFC), a method that enables the high-throughput acquisition and analysis of thousands of light microscopy images (Dunker, 2019; Rees et al., 2022). This method revealed a particularly pronounced increase in cell diameter during the first 2 days after zygote formation (Figure S3). In the following weeks, the cell diameter increased only incrementally. Assuming a cubic relationship between cell volume and diameter, a median cell diameter of 11.4 μm after 28 days corresponds to more than a doubling of the cell volume compared with the initial cell volume with a median diameter of 8.7 μm. The zygote's rapid enlargement in the first 2 days (Figure S3) correlates with the growth of the cell wall seen in the micrographs (Figure 2d), supporting the conclusion that cell wall formation is mainly responsible for the increase in zygote size.

Aside from the development of the zygotic cell wall, the most striking changes in the ultrastructure of *C. reinhardtii* zygotes occurred in the chloroplast. Two days after mating, zygotes possessed an extended chloroplast that resembles the cup-shaped chloroplast of vegetative cells (Figure S4). With increasing zygote age, some thylakoids were preserved, but the chloroplast became less prominent and its shape more variable. In agreement with

a previous report (Cavalier-Smith, 1976), the eyespot was only visible in newly formed zygotes but was absent from any zygotes matured for 2 days or longer (Figure S5). The starch plates surrounding the algal pyrenoid became thinner with increasing maturation time and eventually disappeared to yield a pyrenoid that was completely devoid of the starch sheath after 7 days (Figure 3a; Figure S6). Furthermore, the size of the pyrenoid decreased during zygote maturation, and with a single exception, no pyrenoid was observed in zygotes matured for 21 days or longer (Figure 3b; Figure S4). To uncover the fate of Rubisco, a major constituent of the pyrenoid (Mackinder et al., 2016), proteins were extracted from zygotes after different maturation times and separated by SDS-PAGE. In newly formed zygotes, a prominent band at ~15 kDa was identified as the small subunit of Rubisco (RBCS) by tryptic digestion and liquid chromatography–tandem mass spectrometry (LC–MS/MS) (Table S1). The intensity of the RBCS band decreased with increasing maturation time, indicating that Rubisco is degraded during zygote maturation (Figure S7). The intensity of a major band at ~58 kDa, which contained the large subunit of Rubisco (RbcL; Table S1), showed a similar decrease during zygote maturation as RBCS (Figure S7). In summary, these observations consistently show that the maturing zygote partially degrades its chloroplast on its way to a dormant zygospore.

Pigment content and macromolecular composition are greatly altered

To elucidate the molecular origins of the color change in maturing zygotes, the chlorophylls and carotenoids were extracted and analyzed by high-performance liquid chromatography (HPLC). The overall content of these pigments steadily decreased during the first 2 weeks to stabilize at ~15% of its initial level (Figure 4a). As in vegetative cells of *C. reinhardtii* (García-Cerdán et al., 2020), the pigment profile in early zygotes is dominated by chlorophylls *a* and *b* (Figure 4b; Figures S8, S9; Table S2). Similarly, early zygotes contain carotenes (α-carotene and β-carotene) and the xanthophylls lutein, violaxanthin, neoxanthin/loroxanthin, antheraxanthin, and zeaxanthin. A new group of pigments first detected after 3 days of maturation (Table S2) heralded the profound changes to the pigment composition that occurred 4–14 days after zygote formation. A broad peak with a maximum at ~480 nm in the absorption spectra of the newly formed compounds (Figure S10) agrees with their tentative identification as ketocarotenoids. As a result of the continuing accumulation of these putative ketocarotenoids and the decline of other xanthophylls, carotenes, and chlorophylls, the newly synthesized pigments represented nearly half of the pigments in mature zygospores (Figure 4b). Nevertheless, the chlorophyll retained by zygospores still represented about 25% of the total pigment content.

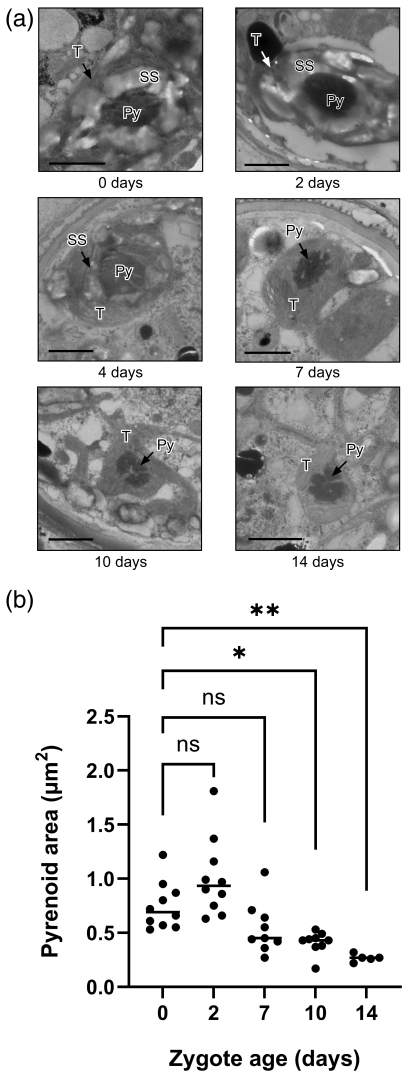

Figure 3. Disappearance of the pyrenoid during zygote maturation. (a) Depletion of the pyrenoid starch sheath (transmission electron micrographs). Scale bar: 1 μm. Py, pyrenoid; SS, starch sheath; T, thylakoid membranes. (b) Decrease in pyrenoid size. As a proxy for pyrenoid size, the pyrenoid area was quantified in TEM cross-sections. The horizontal lines represent mean values ($n = 5$–10). One-way ANOVA was used for statistical comparisons (ns, $P > 0.05$; *, $P \leq 0.05$; **, $P \leq 0.01$). No further timepoints were included as no pyrenoids were observed in zygotes matured for 21 days, and only a single pyrenoid with an area of 0.55 μm^2 was observed in TEM cross-sections after 28 days. The TEM images used to prepare the diagram in (b) are depicted in (a) and Figure S6.

Fourier-transform infrared spectroscopy (FTIR) was employed to assess the changes in the cellular content of proteins, carbohydrates, and lipids (Wagner et al., 2010). Whereas the largest changes in pigment composition were observed after 4–14 days, the macromolecular composition of the *C. reinhardtii* zygotes changed the most in the first few days of maturation. Within 2 days after the formation of zygotes, their protein content dropped from more than 40% to almost 20% (Figure 5a). The absolute protein

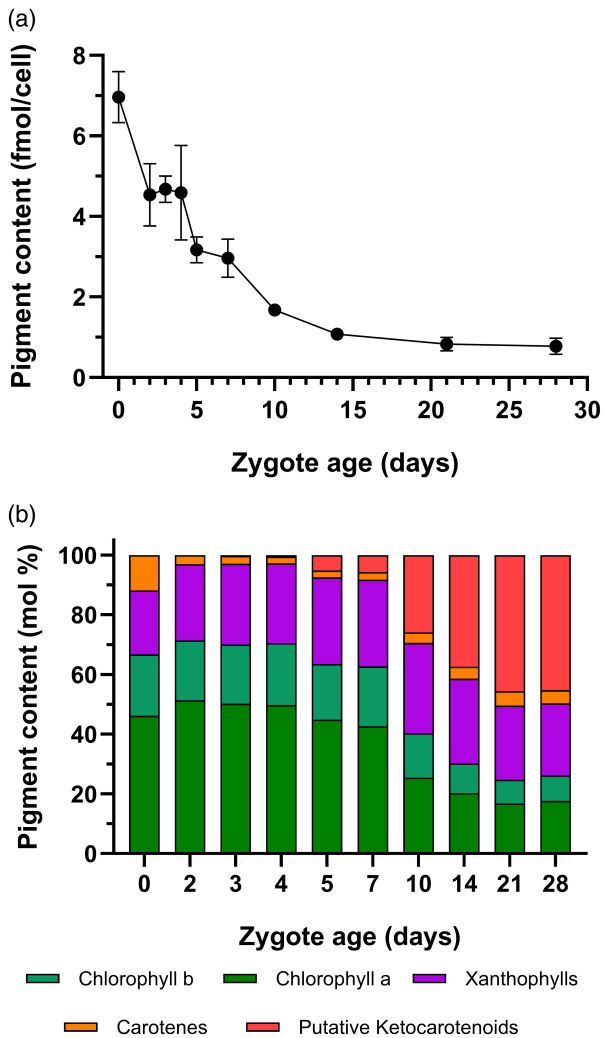

Figure 4. Changes in pigments (chlorophylls and carotenoids) during zygote maturation. (a) Total pigment content. Values indicate the mean ± standard deviation, with $n = 3$ (biological replicates). (b) Relative pigment content. Data result from the mean values of three biological triplicates. Absolute pigment concentrations can be found in Figure S9 and detailed relative values (mean ± standard deviations) and information on individual carotenoids in Table S2.

content decreased as well, albeit to a lesser extent than the relative content (Figure S12). In the first 2 days, the carbohydrates increased from ~ 40% to more than 50%. We then quantified the starch content to test whether starch accumulation accounts for the increase in carbohydrate content. Surprisingly, the starch content was found to decrease from 27% to 7% during maturation (Figure 5b). To elucidate the reason for the discrepancy between the observed increase in total carbohydrates and the depletion of starch, zygote extracts were analyzed by LC–MS. Zygotes started accumulating di- and trisaccharides ($C_{12}H_{22}O_{11}$ and $C_{18}H_{32}O_{16}$, respectively) after 2 days, which peaked a few days later before they decreased again in favor of one or multiple $C_{24}H_{42}O_{21}$ tetrasaccharides (Figure 5c; Figure S13). Due to the possibility of multiple isomers with identical mass and chromatographic co-elution, the detected oligosaccharides remain to be identified. The ion intensities of the tri- and tetrasaccharides increase about 200-fold in mature zygospores compared with newly formed zygotes, suggesting that these oligosaccharides fulfill an important function in the spore.

The lipid content in maturing zygotes rose from ~7% to ~15% in 1 week, corresponding to an approximately twofold accumulation (Figure 5a). An analysis of individual lipids by thin-layer chromatography revealed that the increase in the total lipid content during the first few days after zygote formation is caused by a fast accumulation of triacylglycerols (TAGs) (Figure 5d). In contrast, the lipids that constitute the thylakoid membrane decreased in abundance, which was particularly pronounced for monogalactosyldiacylglycerols (MGDGs). These findings raise the possibility that zygotes can directly synthesize the storage lipid TAG from building blocks derived from the breakdown of thylakoid membranes. A quantitative evaluation of TEM cross-sections indicates that maturing zygotes accumulate cytosolic lipid droplets, although the variability is high and this finding should be verified by further experiments (Figures S4, S14). These lipid droplets probably consist of accumulated TAGs and can serve as a source of energy and carbon as soon as improving conditions allow the zygotes to germinate.

Maturation leads to simultaneous decline in respiration and photosynthesis

To investigate the respiratory and photosynthetic activities of maturing zygotes, we quantified oxygen consumption in darkness and the maximum fluorescence quantum yield of photosystem II (F_v/F_m), respectively. Both vegetative cells and gametes of strain CC-125 (mt^+) showed lower activities than the corresponding cells of strain CC-124 (mt^-), indicative of distinct strain-specific differences (Figure 6a,b; Table S5). Similar to CC-125 gametes, newly formed zygotes exhibited low respiration rates (7.5 nmol h^{-1} per 10^6 cells), which rose to 18 nmol h^{-1} per 10^6 cells after 2 days before they continuously decreased over the following days to level off at low levels (~7 nmol h^{-1} per 10^6 cells) after 7 days (Figure 6c).

Similar to the respiration rate, the low F_V/F_M value of 0.44 observed 3 h after mating increased to 0.64 after 2 days (Figure 6c), a value comparable to the photosynthetic activity of vegetative cells (Table S5). Over the following days, however, F_V/F_M decreased gradually to drop below 0.1 after 10 days of maturation, indicating very low photosynthetic performance. In summary, the temporal changes in respiration and photosynthesis were largely

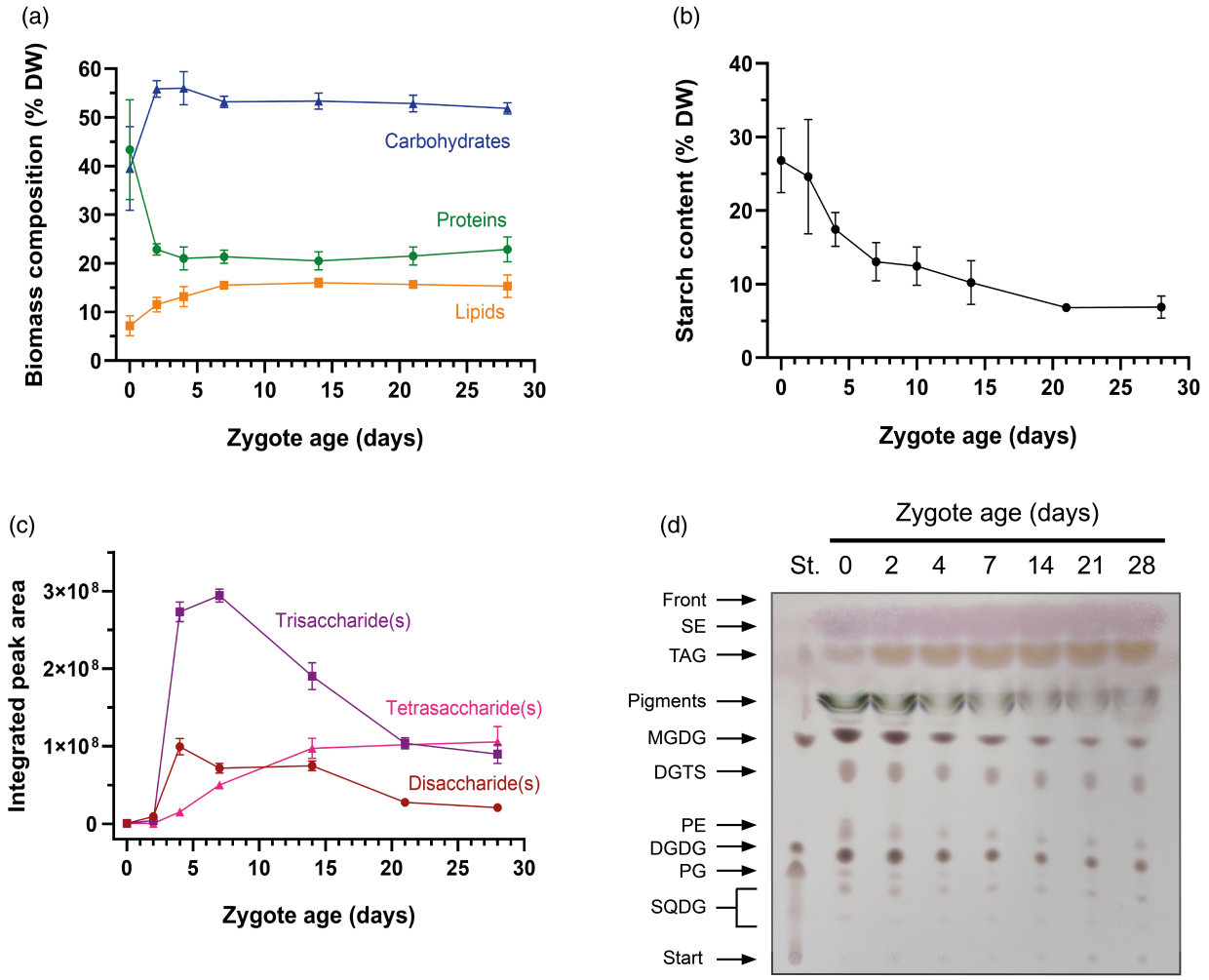

Figure 5. Changes in carbohydrate, lipid, and protein composition during zygote maturation. (a) Macromolecular composition. Values indicate the mean percentage of dry weight (% DW) ± standard deviation, with $n = 6$ (two independent experiments with three biological replicates each). FTIR spectra of newly formed zygotes and 28-day-old zygospores can be found in Figure S11. (b) Starch content. Values indicate the mean ± standard deviation, with $n = 3$ (biological replicates). (c) Oligosaccharide content. No monosaccharides or sugar alcohols were detected (Table S3). Values indicate mean ± standard deviation, with $n = 3$ (biological replicates). Further details on the LC–MS analysis are provided in Figure S13 and Tables S3 and S4. (d) Lipid composition (thin-layer chromatogram). Additional biological replicates are shown in Figure S15. DGDG, digalactosyldiacylglycerol; DGTS, diacylglyceryltrimethylhomoserine; MGDG, monogalactosyldiacylglycerol; PE, phosphatidylethanolamine; PG, phosphatidylglycerol; SE, sterol esters; SQDG, sulfoquinovosyldiacylglycerol; TAG, triacylglycerol.

synchronous, reaching minimal values after 7–10 days of maturation.

Abiotic stress tolerance improves as zygotes mature

Mature zygospores can survive 5 days of desiccation whereas this condition is lethal to vegetative cells (Heimerl et al., 2018). To determine the timepoint when zygotes acquire their desiccation tolerance, they were matured for different periods of time, transferred onto glass fiber filters, and incubated in a desiccator at ~1% relative humidity (Figure 7a). After 5 days of desiccation, the filters were transferred into TAP liquid medium to allow surviving zygotes to germinate, and the time until released vegetative cells formed green cultures was quantified. Only zygotes that had matured for at least 3–4 days were able to survive while younger zygotes did not germinate (Figure 7b; Figure S16). The time for the resulting liquid cultures to turn green decreased with increasing zygote age, suggesting that longer maturation allowed a greater number of zygotes to survive. From these data, we conclude that desiccation tolerance began after 3–4 days and reached its maximum after ~ 14 days.

Using an analogous experimental procedure, maturing zygotes were frozen at −20°C for 5 days (Figure 7a). While freezing completely killed vegetative cells and young zygotes, freezing tolerance emerged 3 days after zygote formation and was fully developed after 7 days (Figure 7c; Figure S17). Albeit freezing tolerance and desiccation

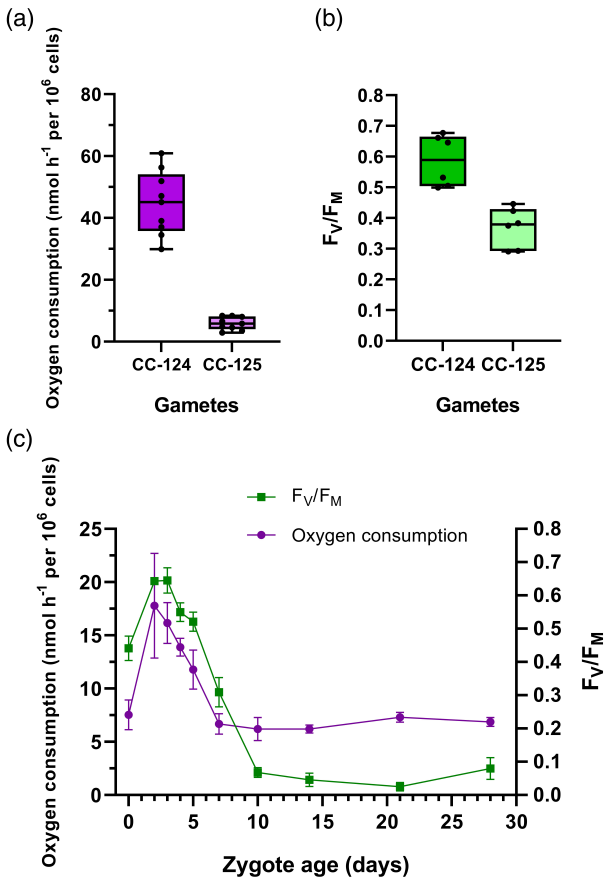

Figure 6. Respiration rate and photosynthetic activity of gametes and maturing zygotes. (a) Respiration rate of gametes. The respiratory activity in strains CC-124 and CC-125 was quantified by measuring oxygen consumption in the dark using a Clark electrode. The boxplots indicate the median (central horizontal line), interquartile range (box), and minimal and maximal values (whiskers), with $n = 9$ (three independent experiments with three biological replicates each). (b) Photosynthetic activity of gametes. The photosynthetic activity was determined as the maximum quantum efficiency of photosystem II (F_v/F_m) of dark-adapted cells. Boxplots are as in (a), with $n = 6$ (two independent experiments with three biological replicates each). (c) Respiration rate and photosynthetic activity during zygote maturation. Values indicate the mean ± standard deviation, with $n = 3$ (biological replicates).

tolerance progressed in parallel, freezing tolerance set in somewhat earlier and was completed earlier than desiccation tolerance.

DISCUSSION

Sexual reproduction occurs in many groups of algae (Umen and Coelho, 2019). While the zygotes of some algal species resume growth after they are formed, the zygotes of other species develop into resting spores (Coleman and Pröschold, 2005). The ability to form zygospores is found in various algal taxa, including unicellular and multicellular species from the classes of Chlorophyceae and Zygnematophyceae (Kirk, 2001; Tsuchikane et al., 2012; Permann et al., 2021). In *C. reinhardtii*, sexual reproduction and particularly zygote maturation have been neglected in comparison to the well-studied vegetative stage. To address this gap and systematically examine the maturation of zygotes into zygospores, we selected TAP-N as a reference medium because it is closely related to the widely used TAP medium and is compatible with zygote maturation under different light conditions. Our experiments demonstrate that the maturation of *C. reinhardtii* zygotes in darkness occurs in a coordinated but asynchronous fashion, consisting of several staggered, partly overlapping processes (Figure 8). For example, the strongest remodeling of the macromolecular composition occurs in the first 2 days (Figure 5a), which is accompanied by a fast decrease in total pigment *content* (Figure 4a); on the other hand, the most drastic changes to pigment *composition* occur in the timeframe 4–14 days after zygote formation (Figure 4b; Figure S9), causing a concomitant color change (Figure 1).

Three different types of electron microscopy (SEM, ESEM, and TEM) consistently revealed an essentially smooth surface of *C. reinhardtii* zygospores (Figure 2a,b; Figure S1). In contrast, zygospores of *Chlamydomonas monoica* and *Chlamydomonas geitleri* possess a reticulate surface ornamentation (Sulek, 1997; VanWinkle-Swift and Rickoll, 1997). These differences suggest that surface structure is genetically determined, but an influence of the environmental conditions cannot be excluded (cf. Sulek, 1997). Cell wall biosynthesis largely coincides with the surge in zygote size during the first 2–4 days of zygote maturation (Figure 2d; Figure S3). At the same time, the intracellular area in TEM cross-sections, which we used as a measure of the volume of the zygote without the cell wall, remains relatively constant (Figure 2d). These results indicate that the formation of the multilayered zygote wall accounts for most of the cell size increase.

In the first few days after zygote formation, the relative amounts of lipids and carbohydrates increase, whereas the relative protein content decreases (Figure 5a). The increase in lipids is caused by TAG accumulation, which is accompanied by the degradation of thylakoid membrane lipids (Figure 5d). These data suggest that the fatty acid and glycerol moieties of lipids important for photosynthesis can be directly converted into storage lipids, a model supported by previous evidence for such a pathway in vegetative cells (Légeret et al., 2016). Furthermore, changes observed during zygote maturation are reminiscent of the response of vegetative cells to nitrogen starvation, which also results in TAG accumulation and a decline in thylakoid lipids (Juergens et al., 2014). Our results further show that three-quarters of the starch are degraded (Figure 5b). Since the cell wall of zygotes contains sugar residues that are part of HRGPs, and possibly other types of carbohydrates (Grief et al., 1987; Woessner and Goodenough, 1989), starch breakdown products may be

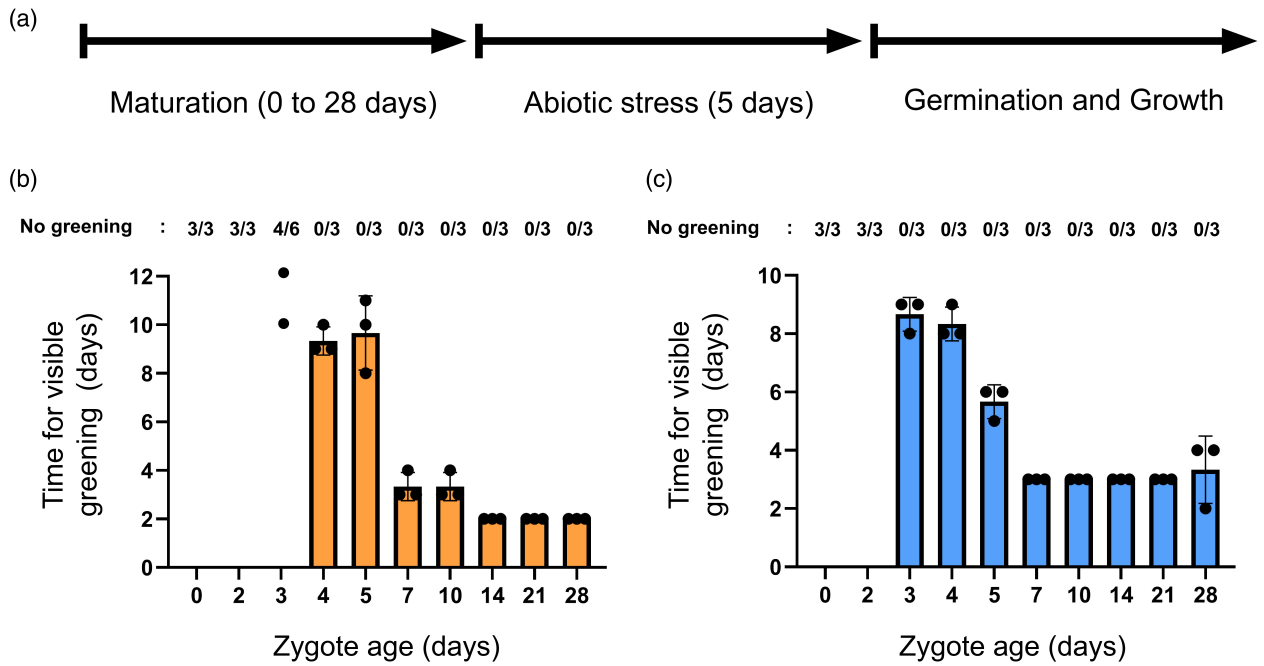

Figure 7. Temporal development of abiotic stress tolerance during zygote maturation. (a) Overview of the experimental procedure. Zygotes were matured for different periods of time, transferred to glass fiber filters, and exposed to abiotic stress (desiccation or freezing) for 5 days. The filter with the zygotes was then rehydrated in 50 mL of TAP medium and the culture incubated at 20°C under 14:10 light/dark cycles (30 μmol photons m^{-2} s^{-1}) and stirring (100 rpm). If zygotes survive the abiotic stress, they are able to germinate after rehydration, and the released vegetative cells can divide to yield a green culture. As a proxy for the number of surviving zygotes, the number of days required for greening was quantified. (B) Recovery after desiccation at ~1% humidity for 5 days. (c) Recovery after freezing at −20°C for 5 days. In (b) and (c), a shorter time until the cultures turn green indicates that more zygotes survived the abiotic stress. The numbers *x*/*y* above each bar indicate that *x* out of a total of *y* cultures (biological replicates) did not turn green. The bars and whiskers indicate the mean ± standard deviation. Photos of the cultures are shown in Figures S16, S17.

channeled into cell wall biosynthesis. It is also possible that the oligosaccharides accumulated by mature zygospores (Figure 5c) are derived from starch. However, the strong increase in total carbohydrates (Figure 5a) and the low photosynthetic activity (Figure 6c) suggest that in the first few days of zygote maturation, carbohydrates are additionally synthesized from acetate.

The low metabolic activity of newly formed zygotes tripled during maturation and then returned to basal levels after approximately 10 days (Figure 6c). This pulse of metabolic activity was similarly observed for both respiratory and photosynthetic activity (Figure 6c). The initial recovery of metabolic activity may be a consequence of the cellular reorganization that follows the fusion of the two gametes. Baldan et al. (1991), who quantified fluorescence induction kinetics in the first 48 h after zygote formation, observed a similar recovery of photosynthesis, which they suggested was a consequence of the fusion of the parental thylakoid membranes after 15 h. In contrast, Aoyama et al. (2009) saw high rates of dark respiration in newly formed zygotes but also found a strong drop over the following days. While the reason for these different results remains unclear, high rates of cellular respiration may be crucial to fuel the zygote's morphological and physiological remodeling at an early stage of maturation. Indeed, respiration reaches its lowest level after 7 days (Figure 6c), which roughly coincides with the completion of the cell wall (Figure 2c,d) and the main phase of TAG accumulation and macromolecular remodeling (Figure 5).

Within 14 days after zygote formation, the total content of pigments decreases to approximately 15% of the initial value (Figure 4a). While the fractions of chlorophylls and most carotenoids decline, the zygote begins to synthesize a new set of carotenoids after 3 days (Figure 4b; Table S2). As described in the accompanying article by Schwarz et al., (2025) these newly formed carotenoids include the ketocarotenoids canthaxanthin, astaxanthin, and 4-ketolutein together with various fatty acid esters of the latter two pigments. Heterologous expression experiments indicated that secondary ketocarotenoids are biosynthesized by a β-carotene ketolase from precursor carotenoids such as β-carotene and zeaxanthin (Huang et al., 2012; Schwarz et al., (2025)). The formation of ketocarotenoids from photosynthetic carotenoids appears to parallel the formation of storage lipids from thylakoid lipids (this work and Schwarz et al., (2025)). The related green alga *Haematococcus pluvialis* accumulates astaxanthin in vegetative spores, so-called aplanospores, where

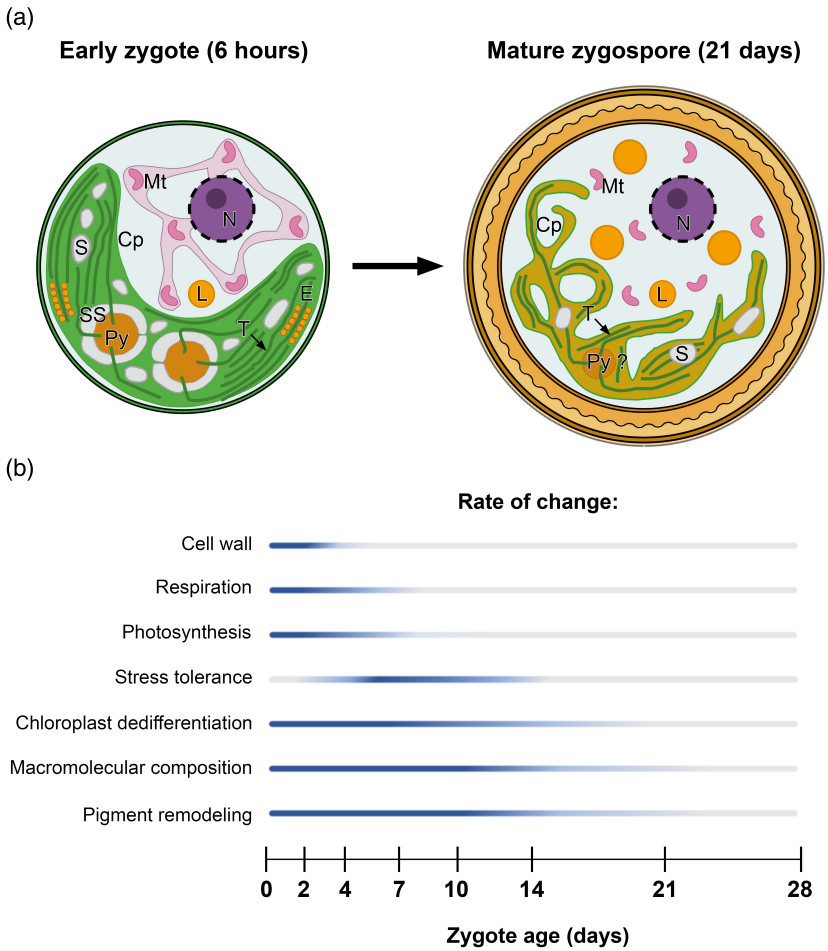

Figure 8. Model for the maturation of *C. reinhardtii* zygotes into dormant zygospores. (a) Morphological and physiological alterations. Major changes include an increase in cell size (Figure 2D; Figure S3), a partial dedifferentiation of the chloroplast that involves the loss of the pyrenoid (Figure 3), a degradation of the eyespot (Figure S5; Cavalier-Smith, 1976), an increase in TAGs and oligosaccharides accompanied by the degradation of starch and chlorophyll (Figures 4, 5), the formation of ketocarotenoids (Figure 4) that may accumulate in cytosolic lipid droplets, and dissolution of mitochondrial networks (Aoyama et al., 2009). Based on a previous analysis (Blank et al., 1978), the schematic zygote after 6 h is depicted with a single nucleus and chloroplast, but two pyrenoids and two eyespots. C, chloroplast; E, eyespot; L, lipid body; Mt, mitochondria; N, nucleus; Py, pyrenoid; S, starch granule; SS; starch sheath; W, cell wall. (b) Timeline of morphological and physiological changes. Dark blue indicates fast changes, light blue slow changes, and gray no changes.

this ketocarotenoid probably functions as an antioxidant (Kobayashi et al., 1997). The observation that *H. pluvialis* stores astaxanthin in cytosolic lipid droplets (Grünewald et al., 2001) and the accumulation of cytosolic lipid droplets in mature zygospores of *C. reinhardtii* (Figures S4, S14; Schwarz et al., (2025)) may point to a similar form of ketocarotenoid storage in the spores of these two species.

Cavalier-Smith (1976) previously reported chloroplast dedifferentiation even though he may not have examined zygotes older than 6 days, and his conclusion was questioned due to possible problems with the fixation of the TEM samples (Goodenough et al., 2023). A partial dedifferentiation of the chloroplast is now supported by our results. The degradation of chlorophyll (Figure 4) and thylakoid membrane lipids (Figure 5d) during zygote maturation correlates with the decrease in photosynthetic activity (Figure 6c) and the partial dedifferentiation of the chloroplast (Figure S4). The starch sheath around the pyrenoid, which is regulated independently of the stromal starch (Kuchitsu et al., 1988), was found to disappear (Figure 3a). Along with the decrease in pyrenoid size over time (Figure 3b), the absence of a pyrenoid in almost all zygotes that are at least 14 days old (Figure S6), and the depletion of Rubisco (Figure S7), this suggests that the pyrenoid is degraded during zygote maturation. All these findings converge into a coherent picture indicating that dormant zygospores have essentially lost the ability for photosynthesis and carbon fixation. When the environmental conditions improve, zygospores begin to ramp up photosynthesis and respiration after approximately 6 h, followed by meiosis around 10 h later (Hommersand and Thimann, 1965; Aoyama et al., 2009; Aoyama et al., 2014). The residual

thylakoids (Figure S4) and small amounts of chlorophyll (Figure 4b) maintained in mature zygospores may prepare them to quit dormancy and respond to the improving conditions quickly.

Isolates of *Chlamydomonas* sp. were shown to survive in dry soil for at least 35 years (Trainor and Gladych, 1995), and it is likely that the zygospore stage is necessary for this survival. In *C. reinhardtii*, desiccation tolerance started to emerge 3–4 days after zygote formation and was fully developed after 2 weeks (Figure 7b). The central layer of the cell wall, which is essential for desiccation tolerance but not for chloroform resistance (Heimerl et al., 2018), is mostly completed after 4 days but appears more elaborate in TEM images after 7 days (Figure 2c). The temporal development of desiccation tolerance is consistent with a critical role of the central layer, but other processes probably also contribute to desiccation tolerance. For example, raffinose, stachyose, and related oligosaccharides play important roles in seed desiccation tolerance in higher plants (Yan et al., 2022), and it seems likely that the oligosaccharides accumulated by zygospores (Figure 5c) may also serve as osmoprotectants. The freezing tolerance of maturing zygotes set in after 3 days and plateaued after 7 days (Figure 7c). Even though many details of the cellular mechanisms responsible for freezing and desiccation tolerance are unknown, the somewhat earlier development of freezing tolerance suggests that different and possibly overlapping mechanisms contribute to these two traits.

In conclusion, *C. reinhardtii* zygotes undergo a profound remodeling during maturation in the dark. Over the course of 10–21 days, the different morphological and physiological changes range from the early macromolecular changes to the acquisition of dormancy and resistance to harsh environmental conditions at a later stage (Figure 8). This comprehensive investigation can serve as a blueprint to elucidate the genes and molecular factors that control zygote maturation.

MATERIALS AND METHODS

Strains, growth conditions, and mating

Vegetative cells of *C. reinhardtii* CC-124 (*mt*$^-$) and CC-125 (*mt*$^+$) were grown on Tris-acetate-phosphate (TAP; Gorman and Levine, 1965) plates containing 2% (w/v) bacto agar (product no. BD 214010, Fisher Scientific) at 20°C under continuous white light (50 μmol photons m^{-2} s^{-1}). Pre-cultures of *C. reinhardtii* CC-124 and CC-125 were grown in 50 mL of TAP medium in 100 mL Erlenmeyer flasks at 20°C, under ~50 μmol photons m^{-2} s^{-1} and 180 rpm for 3 days. Following this period, 500 mL cultures in 1000 mL or 500 mL Erlenmeyer flasks were grown at 60 μmol photons m^{-2} s^{-1}, 20°C and bubbled with air through a 0.22 μm pore filter. After 2–3 days, the biomass was collected using centrifugation at 4°C, 2000 ***g*** for 10 min and resuspended in the same volume of TAP-N medium (TAP medium without NH_4Cl) and again placed at 60 μmol photons m^{-2} s^{-1}, 20°C with air bubbling. After 24 h the biomass was again collected by centrifugation and the density of each gamete culture was adjusted to 5×10^7 cells ml^{-1}, and equal volumes of both cultures were combined. After 2–3 h, a 25-mL serological pipette was used to apply ~1.1 mL aliquots of zygote suspension to TAP-N plates containing 3% (w/v) Difco agar (BD 214530, Fisher Scientific). The plates were allowed to dry under a sterile bench, incubated at 20°C under continuous white light (60 μmol photons m^{-2} s^{-1}) for 24 h, and then wrapped in aluminum foil and incubated at 20°C for various amounts of time (maturation in darkness). To harvest zygotes from the plates, unmated cells were washed away using 2 mL of distilled water, and the remaining unmated cells were pushed aside with a scalpel. Mating efficiency was determined as described (Heimerl et al., 2018) with the following modifications: Biciliated and quadriciliated cells were counted under a Zeiss Axioscop phase-contrast microscope with a 400× magnification and using the differential interference contrast (DIC) field.

For transmission electron microscopy, CC-124 and CC-125 were grown on TAP plates containing 2% (w/v) bacto agar for 4 days at 20°C and 50 μmol photons m^{-2} s^{-1} and then transferred onto TAP-N plates and incubated for 3 days under the same conditions. The gametes of each strain were then suspended in 5 mL of distilled water and placed under 60 μmol photons m^{-2} s^{-1} and 200 rpm for 3 h. Following this period, the cell concentration for both gametes was adjusted to the same concentration, and 7 mL of each gamete were mixed and allowed to mate for 2.5 h before being applied as 330 μL aliquots onto TAP-N + 3% Difco agar plates and allowed to dry under sterile air. The plates were then incubated under 50 μmol photons m^{-2} s^{-1} for 24 h before being wrapped in aluminum foil.

Electron microscopy

For scanning electron microscopy (SEM), zygospore samples were scraped off agar plates together with phosphate-buffered saline (PBS; 10 mM Na_2HPO_4, 1.8 mM KH_2PO_4, 137 mM NaCl, 2.7 mM KCl, pH 7.2) and applied to poly-L-lysine coated slides. The cells were fixed using 2.5% (v/v) glutaraldehyde in PBS for 15 min and subsequently washed with PBS for 10 min. Samples were then dehydrated in an increasing ethanol series (70%, 80%, 90%, 100% (v/v) ethanol), for 10 min at each concentration, followed by 10 min with an 1:1 acetone: ethanol (v/v) solution. After drying the samples by using a critical point dryer (Emitech K850) according to standard conditions, zygotes were imaged with a scanning electron microscope (Zeiss Gemini SEM500) at 1 kV and a secondary electron (SE) detector without coating.

For environmental scanning electron microscopy (ESEM), a piece of agar medium with the zygotes was excised and placed in the sample holder of the environmental scanning electron microscope (Phillips ESEM XL 30 FEG), and the samples were imaged at 20 kV.

For transmission electron microscopy (TEM), zygotes were frozen using high-pressure freezing (HPM 010, Bal-Tec). For freeze substitution (Bal-Tec FSU 010) the fixation solution (0.1% (w/v) uranyl acetate, 0.25% (v/v) glutaraldehyde in acetone) was precooled to −80%, with samples being kept at −80°C for 52 h, −60°C for 6 h, −30°C for 6 h and then kept at −20°C, with all the steps that followed being performed at this temperature unless stated otherwise. Sample infiltration was performed via acetone and dilution series of methyl acrylate: Lowicryl HM20 (25%, 50%, 75%, 100%). Samples were polymerized for 24 h under UV light at −20°C, and for 24 h under UV light at room temperature. Samples were then sectioned (Leica Ultracut S, 70 nm), stained with 1% (w/v) uranyl acetate in distilled water and ultrostain 2 (Leica AC 20), and mounted on Formvar-coated copper 100 and 200

mesh grids. Transmission electron microscopy (Zeiss EM900) was performed at 80 kV together with a water-cooled 1 k slow-scan charged-coupled device (CCD) camera (type 7888, TRS). To quantify (sub-)cellular areas in transmission electron micrographs, the polygon measurement function of ImageSP (version 1.2.8.32) was used. To determine the area occupied by the cell wall, the area enclosed by the cell membrane was subtracted from the total cell area. Several images were acquired for all electron microscopy methods, and representative images are shown.

Imaging flow cytometry

Following the removal of unmated cells, the zygotes were suspended in 4 mL of distilled water. Zygotes matured for 2 days or longer were separated into individual cells using a Sonoplus 4000 ultrasonicator (Bandelin) for 60 s at 60% amplitude (newly formed zygotes would not survive the sonication). Measurements were performed with an ImageStream X Mk II cytometer (Amnis part of Cytek) according to Dunker, 2019. The instrument was equipped with three lasers and two CCD cameras. For the measurements, the laser power was set to 0.5 mW (488 nm laser), 20 mW (561 nm laser including a neutral density filter (ND1.0)), and 0.5 mW (785 nm laser). Brightfield images were recorded via channel Ch01. Measurements were performed with 50 μL of cell suspension at a flow rate of 110 mm s^{-1} using Dulbecco's phosphate-buffered saline (Biowest, X0515-500) as sheath fluid and 600× magnification. A total of 10 000 particles were acquired for each sample.

The data were analyzed with the firmware (IDEAS 6.2, Amnis). In a first step, an AdaptiveErode mask (AdaptiveErode (M01, Ch01, 92)) was created and applied to determine the cell diameter and circularity. Particles larger than a diameter of 5 μm were considered as potential *C. reinhardtii* cells, while particles smaller than 5 μm were mainly debris and calibration beads (Cytek, CN-0440-01), which were excluded from further analysis. In a second step, a biplot of the circularity calculated with the AdaptiveErode mask and the cell area based on Ch01 was used to identify two different populations: (1) particles with an area of approximately 150–1000 μm^2 and a circularity of approximately 0–10 were classified as aggregated cells; and (2) particles with an area of approximately 50–200 μm^2 and a circularity of approximately 3–40 were classified as viable single cells (Figure S18). Single cells (population 2 above) were further analyzed if their side scatter intensity (Ch06) was in the range between approximately 20 000–100 000. The resulting single-cell population was considered for all subsequent analyses. The fine adjustment of regions defining the individual cell populations (gating) was adapted for every measured sample individually based on the cell images.

Protein extraction, separation, and identification

The cells were lysed as described in the section "Pigment analysis" (below) with two modifications: only two rounds of homogenization were performed and 2 mL of 15 mM Tris, 0.1 mM ethylenediaminetetraacetate (EDTA) at pH 7.5 were used as extraction buffer. The lysate was cleared by centrifugation at 11000***g*** and 4°C for 30 min. The total protein concentration was determined using ROTI Quant (Carl Roth, K015.1) with bovine serum albumin (BSA) as a standard. From each extract, 4.2 μg of total protein in sodium dodecyl sulfate (SDS) loading buffer (62.5 mM Tris, pH 6.8, 2% (w/v) SDS, 10% (v/v) glycerol, 0.01% (w/v) bromophenol blue, and 41.7 mM dithiothreitol) were denatured at 95°C for 10 min. The proteins were separated with 4%–15% Mini-PROTEAN TGX gradient gels (Bio-Rad, 456–1084), and the gels were stained with Colloidal Coomassie Blue (Candiano et al., 2004).

For protein identification, gel bands were excised and transferred to reaction tubes. The gel pieces were washed three times with 100 μL of 30% (v/v) acetonitrile in 50 mM ammonium bicarbonate (5 min, 37°C) and dehydrated with 100 μL of acetonitrile (5 min). Proteins were digested with trypsin (5 ng μL^{-1}) in 20 μL 3 mM ammonium bicarbonate (37°C, 4 h). The supernatants were transferred into a new reaction tube and the gel pieces were washed once with 60% (v/v) aqueous acetonitrile containing 0.1% (v/v) formic acid and with acetonitrile (20 μL, 37°C, 5 min). The supernatants were combined.

The samples were diluted in 3% (v/v) aqueous acetonitrile containing 0.1% (v/v) formic acid and analyzed on a nanoACQUITY Ultra Performance LC™ (Waters Corporation) system coupled online to a Q-TOF SYNAPT G2-S*i* instrument (Waters). Peptides were trapped on a nanoACQUITY Symmetry C_{18}-column (internal diameter (ID) 180 μm, length 2 cm, particle diameter 5 μm) at a flow rate of 5 μL min^{-1} (1% (v/v) aqueous acetonitrile containing 0.1% (v/v) formic acid, 6 min) and separated on a C_{18}-BEH 130 column (ID 75 μm, length 10 cm, particle diameter 1.7 μm; 35°C) at a flow rate of 0.3 μL min^{-1} using a linear gradient from 3% to 60% acetonitrile (with 0.1% (v/v) formic acid) over 28 min. The nanoESI source was equipped with a PicoTip Emmitter (New Objective) at a spray voltage of 3 kV; the sampling cone was 30 V, the source offset 80 V, the source temperature 100°C, the cone gas flow 20 L h^{-1}, and nanoflow gas pressure 0.2 bar. Mass spectra were recorded in positive ion mode using a high-definition data-dependent acquisition approach (HD-DDA) for the 10 most intense signals (top ten ions).

LC–MS/MS raw files were processed with PEAKS Studio 10.6 (Bioinformatics Solutions Inc.) using the following parameters: UniProtKB Database with entries from *C. reinhardtii* containing 18 829 entries downloaded on 24 October 2024; enzyme trypsin; maximally three missed cleavage sites; methionine oxidation (+15.9949 Da) as a variable modification; 20 ppm peptide tolerance; and 0.1 Da fragment tolerance. Proteins identified by at least three unique peptides were considered confident.

Pigment analysis

The algal cells (~2.1 × 10^7 cells) were vacuum-filtered onto glass fiber filters. The filters with the cells were placed in a 7 mL Precellys tube along with a glass bead mixture (approximately 1.5–2 mL) and 2 mL of extraction solution. The glass bead mixture consisted of beads with a diameter of 0.25–0.5 mm (Carl Roth, A553.1) and beads with a diameter of 0.75–1.0 mm (Carl Roth, A554.1) in a 3:1 mass ratio, while the extraction solution consisted of 81% (v/v) methanol, 10% (v/v) ethyl acetate, and 9% (v/v) 0.2 M ammonium acetate. Cells were lysed in a Precellys Evolution homogenizer (Bertin Technologies) with two rounds at 6500 rpm for 20 s, with a break of 5 s in between. After disruption, the supernatant was transferred to a 2 mL tube and centrifuged at 15200 ***g*** for 2 min. The supernatant was again transferred to a fresh 2 mL tube and 100 μL were injected into the HPLC column.

Analysis of the pigment extract was performed with an Ultimate 3000 HPLC system (Thermo Fisher Scientific) equipped with a PDA-3000 photodiode array detector. The pigments were separated on a 250/4.6 Nucleosil 120–5 C_{18} reversed-phase column (WICOM) operated at 25°C and a constant flow rate of 1.2 mL min^{-1}. The samples were eluted with a binary gradient consisting of 97.5% (v/v) acetonitrile +2.5% (v/v) 25 mM Tris–HCl, pH 7.5 (eluent A) and

75% (v/v) methanol +25% (v/v) ethyl acetate (eluent B). After 100% eluent A for 18 min, the gradient changed linearly to 100% eluent B over the course of 2 min, and was kept at 100% eluent B for another 15 min. Elution of pigments was monitored at 440 nm, and with the help of the PDA, online absorption spectra in the wavelength range from 400 to 750 nm were recorded. The absorption spectra were used to tentatively identify newly synthesized pigments. The pigments were quantified using calibration factors obtained by the procedure described by Frommolt et al. (2001). For the quantification of putative ketocarotenoids, the average of the calibration factors for the different carotenoids was used.

Analysis of macromolecular composition, starch and lipids

To quantify the content of protein, carbohydrates, and lipids, zygotes from 6 plates (~1.3×10^8 cells in total) were suspended in 30 mL of water for each biological replicate. The cells were collected by centrifugation (3000***g***, 7 min, 20°C) and resuspended in 2 mL of water. About 2 μL of the cell suspension was applied to the surface of a silicon microtiter plate and dried for 10 min at 45°C. The Fourier-transform infrared spectroscopy (FTIR) measurements and evaluations were performed as described (Wagner et al., 2010). It was assumed that proteins, carbohydrates and lipids make up 90% of the total dry weight.

For starch quantification, zygotes from 4 plates (~8.4×10^7 cells in total) were collected as described above. The cell pellets were frozen in liquid nitrogen and lyophilized overnight. 10–20 mg of dried residue were dissolved in 10 mL of 100 mM sodium acetate, pH 5.0, containing 5 mM $CaCl_2$. To solubilize the starch, the samples were autoclaved in a screw cap test tube at 121°C for 1 h. Starch was quantified using the Rapid Total Starch method of the Total Starch Assay Kit (K-TSTA-100A, Megazyme) in accordance with the manufacturer's instructions. To validate starch extraction, an additional lysis step was included by vortexing the zygotes with glass beads (as described below for the lipid extraction) before the sample was autoclaved. As the values for the starch content were very similar to those from the procedure without the additional lysis step, this step was omitted.

For lipid extraction, 4 mL of chloroform/methanol (2:1 volume ratio) were added to a screw cap test tube, along with the frozen *C. reinhardtii* zygote pellet (collected from six zygote plates, approximately 1.3×10^8 cells in total) and the same amount of a glass bead mixture as described under "Pigment analysis". The mixture was vortexed for 20 min. The suspension was then transferred to 2 mL tubes and centrifuged for 2 min at 15200***g*** to remove cell debris. If the pellet was not completely discolored, it was resuspended in chloroform/methanol and vortexed for an additional 5 min. The supernatant was transferred to a new screw cap test tube. 5 M of NaCl was added to obtain an organic-to-aqueous phase volume ratio of 6:4. The mixture was vortexed and centrifuged. The lower organic phase containing the lipids and pigments was collected, transferred into an Eppendorf tube, and dried under a stream of nitrogen. The dried lipids were dissolved in 50 μL chloroform, and 5 μL of extract were separated on a silica thin-layer chromatography plate (HPTLC silica gel 60, 1.05547.0001, Merck) as described (Grünewald et al., 2001). After separation, the plates were sprayed with 5% sulfuric acid and placed at 120°C until the lipid bands became visible.

Oligosaccharide analysis

Frozen zygotes were lysed by vortexing the samples for 45 min in screw cap test tubes with 3 mL extraction buffer (75% methanol and 25% 25 mM ammonium acetate, pH 4.7), the bead mixture described under "Pigment analysis" and five additional glass beads with a diameter of 2–3 mm. The extract was then collected into 2 mL Eppendorf tubes and centrifuged for 30 min at 4°C at 16900***g***. The supernatant was then collected without disturbing the pellet and stored at −20°C. The extracts were analyzed using a Vanquish Horizon UHPLC (Thermo Fisher Scientific) coupled to an Orbitrap Q Exactive Plus mass spectrometer (Thermo Fisher Scientific) with a heated electrospray ion source (HESI). The injection volume was 5 μL and extracts were separated with a Luna NH2 column (150 × 2 mm, 3 μm) (Phenomenex). The column temperature was set to 25°C and the flow rate was 0.25 mL min^{-1}. Solvent A was 25 mM ammonium acetate at pH 9.0 and solvent B was acetonitrile. All the chemicals and solvents used for oligosaccharide analysis were of LC–MS grade. The initial composition was 10% A, followed by a linear increase to 75% A in 8 min, held for 2 min, and changed back to 10% A in 4 min, held for 4 min prior to the next injection. The HESI source was operated in positive mode at 3500 V and the temperature of the ion transfer tube was 250°C. The mass resolution of the Orbitrap was set at 70000 with a mass range of *m/z* 65–750. Peaks were integrated with FreeStyle 1.8 SP2 QF1 (Thermo Fisher Scientific). For each analyte, the peak areas for the $[M + Na]^+$ (*m/z* 365.1054, 527.1583 and 689.2111), $[M + K]^+$ (*m/z* 381.0794, 543.1322 and 705.1850) and $[M + NH_4]^+$ (*m/z* 360.1500, 522.2029, and 684.2557) adducts were combined (expected *m/z* values are indicated in brackets for the di-, tri- and tetrasaccharides, respectively). MS^2 data were obtained by performing full scan data-dependent analyses using an inclusion list with the ions given above. The resolution was set at 17500. An isolation window of ±2 *m/z* units and three normalized collision energies (30, 40, and 50 eV) were used for MS^2 acquisition.

Quantification of respiration and photosynthesis rates

To quantify respiration rates, 4.5×10^7 zygotes or 1.6×10^7 vegetative cells or gametes were filtered onto paper filters (Whatman 2, 1002–055), and the filters placed in the sample chamber of a Light Pipette (Illuminova) coupled with a Clark electrode, and the chamber was filled with 3 mL of TAP medium. Before the measurements, the oxygen saturation was calibrated to 100% using water, and an initial control measurement was performed using TAP medium as a blank. All measurements were performed under constant stirring at 20°C. The oxygen consumption rate was calculated as described (Blache et al., 2011).

To quantify photosynthetic activity, zygotes were suspended in 5 mL of water, while vegetative cells and gametes were collected from liquid cultures. The cells were then transferred to glass fiber filters (MN 85/70, 25 mm, 4 030 025, Macherey-Nagel) by vacuum filtration. The photosynthetic activity was quantified by measuring the maximum quantum efficiency of photosystem II (F_v/F_m) using a chlorophyll fluorometer (Handy PEA+, Hansatech Instruments) with a light pulse of 10 s, 3500 μmol photons m^{-2} s^{-1} and a gain of 0.5 after dark-adapting the zygote samples for 10 min.

Evaluation of zygote stress tolerance

To test desiccation tolerance, zygotes were transferred to glass fiber filters (Whatman GF6, 10 370 003) and incubated in a desiccator without vacuum at 20°C under continuous light (~10 μmol photons m^{-2} s^{-1}) using silica beads as the drying agent to reach approximately 1% relative humidity. To test freezing tolerance, the zygotes were transferred to filters and incubated at −20°C in the dark. Following a stress period of 5 days, the filters were immersed in 50 mL of TAP medium in 100 mL Erlenmeyer flasks and the cultures were incubated at 20°C under white light (30 μmol

photons m^{-2} s^{-1}) with a 14:10 light/dark cycle and stirring (100 rpm). Germination was assessed by daily monitoring the germination of zygotes by visually observing the greening of the cultures.

AUTHOR CONTRIBUTIONS

MC: investigation, formal analysis, visualization, writing - original draft; SK: investigation, methodology, writing – review and editing; SD: methodology, formal analysis, writing – review and editing; AB: investigation, methodology, writing – review and editing; RH: methodology, writing – review and editing; RN: methodology, writing – review and editing; TJ: methodology, writing – review and editing; RG: methodology, writing – review and editing; SS: conceptualization, funding acquisition, writing – original draft.

ACKNOWLEDGEMENTS

We are grateful to Dr. G. Hause and F. Syrowatka for their support with the EM measurements, C. Stehr for critical point drying, and Dr. M. Lohr for helpful comments on the manuscript. Funding by the German Research Foundation (DFG) (grant no. SA 2453/4-1 to S.S.) is gratefully acknowledged. The LC–MS device was funded by the DFG (INST 268/451-1 FUGG) and the Saxon Ministry for Science, Culture and Tourism (SMWK). Open Access funding enabled and organized by Projekt DEAL.

CONFLICT OF INTEREST STATEMENT

The authors declare no conflicts of interest.

DATA AVAILABILITY STATEMENT

All data can be found within the manuscript and the Supporting Information.

SUPPORTING INFORMATION

Additional Supporting Information may be found in the online version of this article.

Figure S1. Scanning electron microscopy (SEM) and environmental scanning electron microscopy (ESEM) images of group of mature *C. reinhardtii* zygospores.

Figure S2. Cell wall of *C. reinhardtii* zygotes matured for 10–28 days in TAP-N medium in the dark.

Figure S3. Increase in cell size during zygote maturation (imaging flow cytometry).

Figure S4. Time course of whole-cell TEM images showing chloroplast dedifferentiation and accumulation of lipid droplets.

Figure S5. Eyespots observed in newly formed zygotes (t = 0 days).

Figure S6. TEM micrographs of pyrenoids found in zygotes matured for different periods of time.

Figure S7. Analysis of zygote proteins by gel electrophoresis (SDS-PAGE).

Figure S8. Selected chromatograms of the pigment analyses in maturing zygotes.

Figure S9. Absolute pigment concentrations in maturing zygotes.

Figure S10. Absorption spectra of putative ketocarotenoid pigments found in zygospores matured for 28 days.

Figure S11. FTIR spectra of newly formed zygotes and of zygospores matured for 28 days.

Figure S12. Absolute protein content of maturing zygotes (FTIR).

Figure S13. Oligosaccharide analysis (extracted ion chromatograms and mass spectra).

Figure S14. Quantification of lipid droplets during zygote maturation.

Figure S15. Changes in lipid composition during zygote maturation (additional replicates).

Figure S16. Zygote viability after desiccation.

Figure S17. Zygote viability after freezing.

Figure S18. Gating strategy used to identify single zygotes by imaging flow cytometry.

Table S1. Identification of proteins in an SDS gel by LC–MS/MS.

Table S2. Detailed composition of the pigment profile of zygotes matured for different periods of time.

Table S3. Theoretical and measured *m*/*z* values (oligosaccharide analysis).

Table S4. Information on the MS^2 spectra of the measured oligosaccharides.

Table S5. Respiration rate and photosynthetic activity of vegetative cells and gametes.

REFERENCES

Akella, S., **Ma, X.**, **Bacova, R.**, **Harmer, Z.P.**, **Kolackova, M.**, **Wen, X.** ***et al.*** (2021) Co-targeting strategy for precise, scarless gene editing with CRISPR/Cas9 and donor ssODNs in *Chlamydomonas*. *Plant Physiology*, **187**, 2637–2655. Available from: https://doi.org/10.1093/plphys/kiab418

Aoyama, H., **Hagiwara, Y.**, **Misumi, O.**, **Kuroiwa, T.** & **Nakamura, S.** (2006) Complete elimination of maternal mitochondrial DNA during meiosis resulting in the paternal inheritance of the mitochondrial genome in *Chlamydomonas* species. *Protoplasma*, **228**, 231–242. Available from: https://doi.org/10.1007/s00709-006-0155-5

Aoyama, H., **Kuroiwa, T.** & **Nakamura, S.** (2009) The dynamic behaviour of mitochondria in living zygotes during maturation and meiosis in *Chlamydomonas reinhardtii*. *European Journal of Phycology*, **44**, 497–507. Available from: https://doi.org/10.1080/09670260903272599

Aoyama, H., **Saitoh, S.**, **Kuroiwa, T.** & **Nakamura, S.** (2014) Comparative analysis of zygospore transcripts during early germination in *Chlamydomonas reinhardtii*. *Journal of Plant Physiology*, **171**, 1685–1692. Available from: https://doi.org/10.1016/j.jplph.2014.07.016

Baldan, B., **Girard-Bascou, J.**, **Wollman, F.-A.** & **Olive, J.** (1991) Evidence for thylakoid membrane fusion during zygote formation in *Chlamydomonas reinhardtii*. *The Journal of Cell Biology*, **114**, 905–915. Available from: https://doi.org/10.1083/jcb.114.5.905

Blache, U., **Jakob, T.**, **Su, W.** & **Wilhelm, C.** (2011) The impact of cell-specific absorption properties on the correlation of electron transport rates measured by chlorophyll fluorescence and photosynthetic oxygen production in planktonic algae. *Plant Physiology and Biochemistry*, **49**, 801–808. Available from: https://doi.org/10.1016/j.plaphy.2011.04.010

Blank, R., **Grobe, B.** & **Arnold, C.-G.** (1978) Time-sequence of nuclear and chloroplast fusions in the zygote of *Chlamydomonas reinhardii*. *Planta*, **138**, 63–64. Available from: https://doi.org/10.1007/BF00392916

Candiano, G., **Bruschi, M.**, **Musante, L.**, **Santucci, L.**, **Ghiggeri, G.M.**, **Carnemolla, B.** ***et al.*** (2004) Blue silver: a very sensitive colloidal Coomassie G-250 staining for proteome analysis. *Electrophoresis*, **25**, 1327–1333. Available from: https://doi.org/10.1002/elps.200305844

Cavalier-Smith, T. (1975) Electron and light microscopy of gametogenesis and gamete fusion in *Chlamydomonas reinhardtii*. *Protoplasma*, **86**, 1–18. Available from: https://doi.org/10.1007/BF01275619

Cavalier-Smith, T. (1976) Electron microscopy of zygospore formation in *Chlamydomonas reinhardtii*. *Protoplasma*, **87**, 297–315. Available from: https://doi.org/10.1007/BF01624002

Coleman, A.W. & **Pröschold, T.** (2005) Control of sexual reproduction in algae in culture (chapter 23). In: Andersen, R.A. (Ed.) *Algal Culturing Techniques*. London: Academic Press, pp. 389–397.

Craig, R.J., **Gallaher, S.D.**, **Shu, S.**, **Salomé, P.A.**, **Jenkins, J.W.**, **Blaby-Haas, C.E.** ***et al.*** (2023) The *Chlamydomonas* genome project, version 6: reference assemblies for mating-type *plus* and *minus* strains reveal extensive structural mutation in the laboratory. *The Plant Cell*, **35**, 644–672. Available from: https://doi.org/10.1093/plcell/koac347

Crozet, P., **Navarro, F.J.**, **Willmund, F.**, **Mehrshahi, P.**, **Bakowski, K.**, **Lauersen, K.J.** ***et al.*** (2018) Birth of a photosynthetic chassis: a MoClo toolkit enabling synthetic biology in the microalga *Chlamydomonas reinhardtii*. *ACS Synthetic Biology*, **7**, 2074–2086. Available from: https://doi.org/10.1021/acssynbio.8b00251

Dunker, S. (2019) Hidden secrets behind dots: improved phytoplankton taxonomic resolution using high-throughput imaging flow cytometry. *Cytometry, Part A*, **95**, 854–868. Available from: https://doi.org/10.1002/cyto.a.23870

Ferris, P.J., **Armbrust, E.V.** & **Goodenough, U.W.** (2002) Genetic structure of the mating-type locus of *Chlamydomonas reinhardtii*. *Genetics*, **160**, 181–200. Available from: https://doi.org/10.1093/genetics/160.1.181

Ferris, P.J., **Waffenschmidt, S.**, **Umen, J.G.**, **Lin, H.**, **Lee, J.-H.**, **Ishida, K.** ***et al.*** (2005) *Plus* and *minus* sexual agglutinins from *Chlamydomonas reinhardtii*. *Plant Cell*, **17**, 597–615. Available from: https://doi.org/10.1105/tpc.104.028035

Findinier, J. & **Grossman, A.R.** (2023) Chlamydomonas: fast tracking from genomics. *Journal of Phycology*, **59**, 644–652. Available from: https://doi.org/10.1111/jpy.13356

Ford, S.A., **Craig, R.J.** & **Ness, R.W.** (2023) A novel method for identifying *Chlamydomonas reinhardtii* (Chlorophyta) and closely related species from nature. *Journal of Phycology*, **59**, 281–288. Available from: https://doi.org/10.1111/jpy.13306

Frommolt, R., **Goss, R.** & **Wilhelm, C.** (2001) The de-epoxidase and epoxidase reactions of *Mantoniella squamata* (Prasinophyceae) exhibit different substrate-specific reaction kinetics compared to spinach. *Planta*, **213**, 446–456. Available from: https://doi.org/10.1007/s004250100589

García-Cerdán, J.G., **Schmid, E.M.**, **Takeuchi, T.**, **McRae, I.**, **McDonald, K.L.**, **Yordduangjun, N.** ***et al.*** (2020) Chloroplast Sec14-like 1 (CPSFL1) is essential for normal chloroplast development and affects carotenoid accumulation in *Chlamydomonas*. *Proceedings of the National Academy of Sciences of the United States of America*, **117**, 12452–12463. Available from: https://doi.org/10.1073/pnas.1916948117

Goodenough, U. & **Lee, J.-H.** (2023) Cell walls (chapter 3). In: Goodenough, U. (Ed.) *The Chlamydomonas Sourcebook*, Vol. **1**, 3rd edition. London: Academic Press.

Goodenough, U., **Lee, J.-H.** & **Snell, W.J.** (2023) The sexual cycle (chapter 9). In: Goodenough, U. (Ed.) *The Chlamydomonas Sourcebook*, Vol. **1**, 3rd edition. London: Academic Press.

Gorman, D.S. & **Levine, R.P.** (1965) Cytochrome *f* and plastocyanin: their sequence in the photosynthetic electron transport chain of *Chlamydomonas reinhardtii*. *Proceedings of the National Academy of Sciences of the United States of America*, **54**, 1665–1669. Available from: https://doi.org/10.1073/pnas.54.6.1665

Grief, C., **O'Neill, M.A.** & **Shaw, P.J.** (1987) The zygote cell wall of *Chlamydomonas reinhardtii*: a structural, chemical and immunological approach. *Planta*, **170**, 433–445. Available from: https://doi.org/10.1007/BF00402977

Grünewald, K., **Hirschberg, J.** & **Hagen, C.** (2001) Ketocarotenoid biosynthesis outside of plastids in the unicellular green alga *Haematococcus pluvialis*. *The Journal of Biological Chemistry*, **276**, 6023–6029. Available from: https://doi.org/10.1074/jbc.M006400200

Hamaji, T., **Lopez, D.**, **Pellegrini, M.** & **Umen, J.** (2016) Identification and characterization of a *cis*-regulatory element for zygotic gene expression in *Chlamydomonas reinhardtii*. *G3 (Bethesda)*, **6**, 1541–1548. Available from: https://doi.org/10.1534/g3.116.029181

Heimerl, N., **Hommel, E.**, **Westermann, M.**, **Meichsner, D.**, **Lohr, M.**, **Hertweck, C.** ***et al.*** (2018) A giant type I polyketide synthase participates in zygospore maturation in *Chlamydomonas reinhardtii*. *The Plant Journal*, **95**, 268–281. Available from: https://doi.org/10.1111/tpj.13948

Hommersand, M.H. & **Thimann, K.V.** (1965) Terminal respiration of vegetative cells and zygospores in *Chlamydomonas reinhardtii*. *Plant Physiology*, **40**, 1220–1227. Available from: https://doi.org/10.1104/pp.40.6.1220

Huang, J., **Zhong, Y.**, **Sandmann, G.**, **Liu, J.** & **Chen, F.** (2012) Cloning and selection of carotenoid ketolase genes for the engineering of high-yield astaxanthin in plants. *Planta*, **236**, 691–699. Available from: https://doi.org/10.1007/s00425-012-1654-6

Huang, K. & **Beck, C.F.** (2003) Phototropin is the blue-light receptor that controls multiple steps in the sexual life cycle of the green alga *Chlamydomonas reinhardtii*. *Proceedings of the National Academy of Sciences of the United States of America*, **100**, 6269–6274. Available from: https://doi.org/10.1073/pnas.0931459100

Joo, S., **Kariyawasam, T.**, **Kim, M.**, **Jin, E.**, **Goodenough, U.** & **Lee, J.-H.** (2022) Sex-linked deubiquitinase establishes uniparental transmission of chloroplast DNA. *Nature Communications*, **13**, 1133. Available from: https://doi.org/10.1038/s41467-022-28807-6

Joo, S., **Nishimura, Y.**, **Cronmiller, E.**, **Hong, R.H.**, **Kariyawasam, T.**, **Wang, M.H.** ***et al.*** (2017) Gene regulatory networks for the haploid-to-diploid transition of *Chlamydomonas reinhardtii*. *Plant Physiology*, **175**, 314–332. Available from: https://doi.org/10.1104/pp.17.00731

Juergens, M.T., **Deshpande, R.R.**, **Lucker, B.F.**, **Park, J.-J.**, **Wang, H.**, **Gargouri, M.** ***et al.*** (2014) The regulation of photosynthetic structure and function during nitrogen deprivation in *Chlamydomonas reinhardtii*. *Plant Physiology*, **167**, 558–573. Available from: https://doi.org/10.1104/pp.114.250530

Kirk, D.L. (2001) Germ-soma differentiation in *Volvox*. *Developmental Biology*, **238**, 213–223. Available from: https://doi.org/10.1006/dbio.2001.0402

Kobayashi, M., **Kakizono, T.**, **Nishio, N.**, **Nagai, S.**, **Kurimura, Y.** & **Tsuji, Y.** (1997) Antioxidant role of astaxanthin in the green alga *Haematococcus pluvialis*. *Applied Microbiology and Biotechnology*, **48**, 351–356. Available from: https://doi.org/10.1007/s002530051061

Kuchitsu, K., **Tsuzuki, M.** & **Miyachi, S.** (1988) Changes of starch localization within the chloroplast induced by changes in CO_2 concentration during growth of *Chlamydomonas reinhardtii*: independent regulation of pyrenoid starch and stroma starch. *Plant & Cell Physiology*, **29**, 1269–1278. Available from: https://doi.org/10.1093/oxfordjournals.pcp.a077635

Kurvari, V., **Grishin, N.V.** & **Snell, W.J.** (1998) A gamete-specific, sex-limited homeodomain protein in *Chlamydomonas*. *The Journal of Cell Biology*, **143**, 1971–1980. Available from: https://doi.org/10.1083/jcb.143.7.1971

Lee, J.-H., **Lin, H.**, **Joo, S.** & **Goodenough, U.** (2008) Early sexual origins of homeoprotein heterodimerization and evolution of the plant KNOX/BELL family. *Cell*, **133**, 829–840. Available from: https://doi.org/10.1016/j.cell.2008.04.028

Légeret, B., **Schulz-Raffelt, M.**, **Nguyen, H.M.**, **Auroy, P.**, **Beisson, F.**, **Peltier, G.** ***et al.*** (2016) Lipidomic and transcriptomic analyses of *Chlamydomonas reinhardtii* under heat stress unveil a direct route for the conversion of membrane lipids into storage lipids. *Plant, Cell & Environment*, **39**, 834–847. Available from: https://doi.org/10.1111/pce.12656

Li, X., **Patena, W.**, **Fauser, F.**, **Jinkerson, R.E.**, **Saroussi, S.**, **Meyer, M.T.** ***et al.*** (2019) A genome-wide algal mutant library and functional screen identifies genes required for eukaryotic photosynthesis. *Nature Genetics*, **51**, 627–635. Available from: https://doi.org/10.1038/s41588-019-0370-6

Lopez, D., **Hamaji, T.**, **Kropat, J.**, **De Hoff, P.**, **Morselli, M.**, **Rubbi, L.** ***et al.*** (2015) Dynamic changes in the transcriptome and methylome of *Chlamydomonas reinhardtii* throughout its life cycle. *Plant Physiology*, **169**, 2730–2743. Available from: https://doi.org/10.1104/pp.15.00861

Mackinder, L.C.M., **Meyer, M.T.**, **Mettler-Altmann, T.**, **Chen, V.K.**, **Mitchell, M.C.**, **Caspari, O.** ***et al.*** (2016) A repeat protein links rubisco to form the eukaryotic carbon-concentrating organelle. *Proceedings of the National Academy of Sciences of the United States of America*, **113**, 5958–5963. Available from: https://doi.org/10.1073/pnas.1522866113

Merchant, S.S., **Prochnik, S.E.**, **Vallon, O.**, **Harris, E.H.**, **Karpowicz, S.J.**, **Witman, G.B.** ***et al.*** (2007) The *Chlamydomonas* genome reveals the evolution of key animal and plant functions. *Science*, **318**, 245–251. Available from: https://doi.org/10.1126/science.1143609

Müller, N., **Wenzel, S.**, **Zou, Y.**, **Künzel, S.**, **Sasso, S.**, **Weiß, D.** ***et al.*** (2017) A plant cryptochrome controls key features of the *Chlamydomonas* circadian clock and its life cycle. *Plant Physiology*, **174**, 185–201. Available from: https://doi.org/10.1104/pp.17.00349

Pan, J. & **Snell, W.J.** (2005) *Chlamydomonas* shortens its flagella by activating axonemal disassembly, stimulating IFT particle trafficking, and blocking anterograde cargo loading. *Developmental Cell*, **9**, 431–438. Available from: https://doi.org/10.1016/j.devcel.2005.07.010

Pasquale, S.M. & **Goodenough, U.W.** (1987) Cyclic AMP functions as a primary sexual signal in gametes of *Chlamydomonas reinhardtii*. *The*

Journal of Cell Biology, **105**, 2279–2292. Available from: https://doi.org/10.1083/jcb.105.5.2279

Permann, C., **Herburger, K.**, **Niedermeier, M.**, **Felhofer, M.**, **Gierlinger, N.** & **Holzinger, A.** (2021) Cell wall characteristics during sexual reproduction of *Mougeotia* sp. (Zygnematophyceae) revealed by electron microscopy, glycan microarrays and RAMAN spectroscopy. *Protoplasma*, **258**, 1261–1275. Available from: https://doi.org/10.1007/s00709-021-01659-5

Rees, P., **Summers, H.D.**, **Filby, A.**, **Carpenter, A.E.** & **Doan, M.** (2022) Imaging flow cytometry. *Nature Reviews Methods Primers*, **2**, 86. Available from: https://doi.org/10.1038/s43586-022-00167-x

Salomé, P.A. & **Merchant, S.S.** (2019) A series of fortunate events: introducing *Chlamydomonas* as a reference organism. *Plant Cell*, **31**, 1682–1707. Available from: https://doi.org/10.1105/tpc.18.00952

Sasso, S., **Stibor, H.**, **Mittag, M.** & **Grossman, A.R.** (2018) From molecular manipulation of domesticated *Chlamydomonas reinhardtii* to survival in nature. *eLife*, **7**, e39233. Available from: https://doi.org/10.7554/eLife.39233

Schwarz, S., **Bauch, M.**, **Schmitt, V.**, **Hallmann, A.** & **Lohr, M.** (2025) *Chlamydomonas reinhardtii, Volvox carteri* and related green algae accumulate ketocarotenoids not in vegetative cells but in zygospores. *The Plant Journal*, (accepted).

Sulek, J. (1997) Variations of the surface sculpture and cell wall ultrastructure of the zygospores in *Chlamydomonas geitleri* (Chlorophyta). *Botanica Acta: Journal of the German Botanical Society*, **110**, 444–451. Available from: https://doi.org/10.1111/j.1438-8677.1997.tb00661.x

Suzuki, L. & **Johnson, C.H.** (2002) Photoperiodic control of germination in the unicell *Chlamydomonas*. *Naturwissenschaften*, **89**, 214–220. Available from: https://doi.org/10.1007/s00114-002-0302-6

Suzuki, L., **Woessner, J.P.**, **Uchida, H.**, **Kuroiwa, H.**, **Yuasa, Y.**, **Waffenschmidt, S.** ***et al.*** (2000) A zygote-specific protein with hydroxyproline-rich glycoprotein domains and lectin-like domains involved in the assembly of the cell wall of *Chlamydomonas reinhardtii* (Chlorophyta). *Journal of Phycology*, **36**, 571–583. Available from: https://doi.org/10.1046/j.1529-8817.2000.99112.x

Trainor, F.R. & **Gladych, R.** (1995) Survival of algae in a desiccated soil: a 35-year study. *Phycologia*, **34**, 191–192. Available from: https://doi.org/10.2216/i0031-8884-34-3-191.1

Tsuchikane, Y., **Tsuchiya, M.**, **Hindák, F.**, **Nozaki, H.** & **Sekimoto, H.** (2012) Zygospore formation between homothallic and heterothallic strains of *Closterium*. *Sexual Plant Reproduction*, **25**, 1–9. Available from: https://doi.org/10.1007/s00497-011-0174-z

Umen, J. & **Coelho, S.** (2019) Algal sex determination and the evolution of anisogamy. *Annual Review of Microbiology*, **73**, 267–291. Available from: https://doi.org/10.1146/annurev-micro-020518-120011

VanWinkle-Swift, K.P. & **Rickoll, W.L.** (1997) The zygospore wall of *Chlamydomonas monoica* (Chlorophyceae): morphogenesis and evidence for the presence of sporopollenin. *Journal of Phycology*, **33**, 655–665. Available from: https://doi.org/10.1111/j.0022-3646.1997.00655.x

Wagner, H., **Liu, Z.**, **Langner, U.**, **Stehfest, K.** & **Wilhelm, C.** (2010) The use of FTIR spectroscopy to assess quantitative changes in the biochemical composition of microalgae. *Journal of Biophotonics*, **3**, 557–566. Available from: https://doi.org/10.1002/jbio.201000019

Woessner, J.P. & **Goodenough, U.W.** (1989) Molecular characterization of a zygote wall protein: an extensin-like molecule in *Chlamydomonas reinhardtii*. *Plant Cell*, **1**, 901–911. Available from: https://doi.org/10.1105/tpc.1.9.901

Yan, S., **Liu, Q.**, **Li, W.**, **Yan, J.** & **Fernie, A.R.** (2022) Raffinose family oligosaccharides: crucial regulators of plant development and stress responses. *Critical Reviews in Plant Sciences*, **41**, 286–303. Available from: https://doi.org/10.1080/07352689.2022.2111756

Zou, Y., **Wenzel, S.**, **Müller, N.**, **Prager, K.**, **Jung, E.-M.**, **Kothe, E.** ***et al.*** (2017) An animal-like cryptochrome controls the *Chlamydomonas* sexual cycle. *Plant Physiology*, **174**, 1334–1347. Available from: https://doi.org/10.1104/pp.17.00493